Research Article | Vol. 10, No. 7 | 1 Jul 2019 | BIOMEDICAL OPTICS EXPRESS 3533
Biomedical Optics EXPRESS

Identifying non-muscle-invasive and muscle-invasive bladder cancer based on blood serum surface-enhanced Raman spectroscopy

SHUO CHEN,[1,2,6] SHANSHAN ZHU,[1,6] XIAOYU CUI,[1,2] WENBIN XU,[3] CHUIZE KONG,[4,7] ZHE ZHANG,[4,8] AND WEI QIAN[5]

[1]*Sino-Dutch Biomedical and Information Engineering School, Northeastern University, Shenyang, 110169, China*
[2]*Key Laboratory of Data Analytics and Optimization for Smart Industry (Northeastern University), Ministry of Education, China*
[3]*Science and Technology on Optical Radiation Laboratory, Beijing, 110854, China*
[4]*Department of Urology, First Affiliated Hospital, China Medical University, Shenyang, 110001, China*
[5]*College of Engineering, University of Texas at El Paso, El Paso, 79968, USA*
[6]*Authors contributed equally to this work*
[7]*kongchuize_cmu@sina.cn*
[8]*zhangzhe@cmu1h.com*

Abstract: The assessment of the muscle invasion of bladder cancer typically plays a crucial role in therapeutic decision-making and has significant impacts on the recurrence rate and survival rate. Although histopathology is sufficiently accurate and usually served as the gold standard for bladder cancer diagnosis, it is invasive, time-consuming, and requires intensive sample preparation by a well-trained pathologist to achieve an optimal diagnosis. Therefore, a fast and noninvasive method to accurately identify non-muscle-invasive bladder cancer (NMIBC) and muscle-invasive bladder cancer (MIBC) is in demand. In this study, the SERS technique combined with the PLS-LDA method based on a small amount of blood serum samples is employed to distinguish healthy volunteers, NMIBC, and MIBC patients. According to the results, the overall diagnostic accuracy is 93.3%. The diagnostic accuracies are 97.8% and 93.2% for healthy versus bladder cancer groups and NMIBC versus MIBC groups, respectively. Therefore, the proposed method has demonstrated excellent performance on accurately identifying muscle invasion of bladder cancer, which can assist timely diagnosis and proper treatment for bladder cancer patients.

© 2019 Optical Society of America under the terms of the OSA Open Access Publishing Agreement

1. Introduction

Bladder cancer is a common urological malignancy involving the urothelium, which has become the 10th most common cancer worldwide [1]. In recent years, an estimated 549,000 new cases of bladder cancer were diagnosed, leading to approximately 188,000 deaths every year [2]. At its initial stage, around 70% of patients suffer from non-muscle-invasive bladder cancer (NMIBC), whereas the remaining suffer from muscle-invasive bladder cancer (MIBC) [3]. NMIBC is confined to the mucosa and/or with invasion only into the underlying lamina propria, whereas MIBC typically invades into deeper layers of the bladder, such as muscle, bladder wall or other tissues surrounding the bladder [4]. In clinical practice, it has been demonstrated that the occurrence of muscle invasion is an important prognostic factor in bladder cancer and plays a crucial role in therapeutic decision-making. The gold-standard treatment for NMIBC patients is the transurethral resection of bladder tumor, while that for MIBC patients is radical cystectomy [5]. The choice of treatment is important, because it has significant impacts on the recurrence rate and survival rate of bladder cancer patients. Although more than half of NMIBC patients show recurrence within five years after initial resections and about 10%-15% of recurrences accompany with features of progression, recent

#365302 https://doi.org/10.1364/BOE.10.003533
Journal © 2019 Received 16 Apr 2019; revised 16 Jun 2019; accepted 18 Jun 2019; published 24 Jun 2019

Biomedical Optics EXPRESS

reports have shown that the 5-year survival rate is approximately 90% for NMIBC patients [1]. In contrast, a much higher rate of metastatic disease and poor 5-year survival rate of only 50% are observed among MIBC patients [6]. Therefore, early and accurate identification of NMIBC and MIBC is with significant importance for a timely decision on precise treatment and therapy, in which the survival rate of bladder cancer patients can be significantly improved.

Currently, the primary clinical methods for evaluating NMIBC and MIBC include cystoscopy, bladder imaging and histopathological diagnosis. Cystoscopy is the most frequently used method for NMIBC diagnosis, but it is invasive and usually associated with patients' unpleasantness, and it can only offer a relative low diagnostic accuracy of approximately 71% [4,7]. Bladder imaging usually restricts its clinical applications due to the potential allergy to contrast agents, and its diagnostic accuracy is only around 76% [8,9]. Ultrasonography often fails to detect primary tumors of NMIBC due to its low spatial resolution and the staging accuracy is only about 78% [10]. Although the development of computed tomography (CT) and magnetic resonance imaging (MRI) brings a more accurate and sensitive bladder cancer diagnosis, the reported accuracy of CT and MRI for staging bladder cancer varies from 55% to 89% [11–14], in which the diagnostic accuracy relies heavily on the characteristics of the medical imaging systems and the radiologists' experience. Histopathology is typically served as the gold standard for bladder cancer diagnosis. However, it is invasive and time-consuming, in which intensive sample preparation by a well-trained pathologist is required to achieve an optimal diagnosis [15]. Although many urinary molecular markers such as bladder tumor antigen (BTA), nuclear matrix protein-22 (NMP22), microsatellite analysis and microRNAs (miRNAs) have been developed in recent years [16,17], all those markers are confronted with varying sensitivity, specificity and high false positive rate, thus none of them has been accepted as a standard clinical diagnostic examination [18]. Therefore, a fast, sensitive and noninvasive diagnostic technique for identifying muscle invasion of bladder cancer would be of imperative clinical value, in which therapy plans can be made timely and rationally for individual patients.

Raman spectroscopy is a fast, non-destructive and label-free technique that can provide spectroscopic fingerprint information about molecular composition and structure based on the measurement of inelastic scattering between monochromatic photons and vibrating molecules. In the past two decades, it has demonstrated great potential as a promising diagnostic tool for cancer detection, by examination on cell, tissue or body fluid like saliva, urine and blood [19]. For those biological samples, surface-enhanced Raman spectroscopy (SERS) is often employed to enhance the inherent weak Raman signal [20,21], and a large enhancement factor of 10^5 to 10^{14} can typically be achieved. The SERS enhancement effect is primarily contributed by electromagnetic enhancement and chemical enhancement. The former is caused by localized surface plasmon resonance excited on the surface of metal with a weak interaction between metal and molecules [22], while the latter is caused by the charge transferring between metal and molecules [23]. In particular, SERS measurement on blood samples is most frequently used as a label-free and noninvasive method in early cancer diagnosis with high sensitivity and shows significant advantages in convenient and repeatable collections from patients [24]. Bladder cancer, as one of the highest recurrence rates and the most malignant tumors, its early detection, diagnosis and treatment are imperative for optimal clinical outcomes. Thus, many studies have been performed on early diagnosis of bladder cancer based on SERS technique. Li *et.al* applied SERS technique on human blood serum to classify bladder cancer patients and healthy volunteers with the diagnostic sensitivity of 90.9% and specificity of 100% [25]. Zhang *et.al* acquired blood serum SERS spectra from healthy volunteers, low-grade and high-grade bladder cancer patients, and the diagnostic accuracies of 96.4% and 95.4% were achieved when differentiating healthy subjects versus bladder cancer patients and low-grade versus high-grade bladder cancer patients, respectively [26]. Although blood serum SERS has demonstrated excellent performance on detecting

Biomedical Optics EXPRESS

bladder cancer and identifying low-grade and high-grade bladder cancer patients, the characterization of muscle invasion of bladder cancer has not yet been investigated. In clinical practice, the occurrence of muscle invasion is one of the most important factors for making therapy plans, which has great impact on the recurrence rate and survival rate of bladder cancer patients.

In this study, the blood serum SERS spectra were collected from the mixture of 2µl silver colloid and only 2µl blood serum from each healthy volunteer, NMIBC and MIBC patient, and significant biochemical changes were observed among those different groups. Furthermore, the partial least square (PLS) analysis followed by linear discriminate analysis (LDA) was used to distinguish healthy, NMIBC and MIBC patients. Based on the results, the overall diagnostic accuracy was 93.3%, and the integrated area under the receiver operating characteristic (ROC) curve were 0.987 for healthy subjects versus bladder cancer patients and 0.983 for NMIBC versus MIBC patients, respectively. Compared to the conventional clinical methods, the proposed blood serum SERS method has demonstrated its potential for fast, accurate and noninvasive assessment of muscle invasion of bladder cancer; thus, rational therapy plans can be made timely and the survival rate of bladder cancer patients can be improved significantly.

2. Materials and methods

2.1 Blood serum sample collection, preparation and SERS measurements

In this study, blood serum samples were collected from 30 healthy volunteers and 60 bladder cancer patients (including 28 NMIBC cases and 32 MIBC cases) from the department of urology in the First Affiliated Hospital of China Medical University. Patients with other systemic diseases except bladder cancer have been excluded and the bladder cancer diagnoses were made based on the histopathology examinations. Ethical approval was obtained from the medical ethics committee of the First Affiliated Hospital of China Medical University, and informed consents were signed by all patients in order to perform human blood research. After 12 hours of overnight fasting, 3 ml peripheral blood sample was collected from each study subject between 7:00-8:00am. The blood samples were then centrifuged at 3000 rpm at 4° C for 10 minutes, and serum was obtained by collecting the supernatant. Then, these serum samples were promptly stored at −80°C until SERS measurements were performed.

For SERS, Lee-Meisel method, i.e. reduction of silver nitrate with trisodium citrate, is one of the most frequently used silver colloids synthesis methods. However, the long heating duration and large volume solution along with uneven heating sometimes lead to various sizes of nanoparticles [27]. In our study, an advanced method by using microwave heating and gradually adding trisodium citrate solution into silver nitrate solution was employed for synthesizing silver colloids, in which much shorter heating duration is needed and the efficiency of SERS enhancement effect can be improved [28,29]. More specifically, 30 mg of $AgNO_3$ was dissolved with 150 ml deionized water and heated to boiling. 1 ml trisodium citrate solution with a concentration of 1% was slowly added into the solution, and then the solution was heated to boiling again. This procedure was repeated 4 times until a total of 4 ml trisodium citrate solution was fully added into the $AgNO_3$ solution, and then the silver colloid solution was cooled at the room temperature. 4ml silver colloid solution was taken and concentrated by centrifugation at 10,000rpm for 8 minutes, discarding 3.5ml of the supernatant. Subsequently, 2µl silver colloid was mixed with 2µl blood serum in 1:1 proportion. Then, the mixture was stirred on an oscillator for five minutes and was incubated at room temperature for 2 hours before taking SERS measurements. A drop of the mixture was transferred onto an aluminum substrate and air dried for optimal SERS measurements. The silver colloidal particles were characterized by transmission electron microscopy (TEM) and UV/visible absorption spectroscopy. The TEM photograph of the silver colloid mixed with blood serum and the absorption spectrum of the silver colloid are shown in Fig. 1. The

Biomedical Optics EXPRESS

silver nanoparticles are spherical with a diameter of approximately 20 to 50 nm, and the maximum absorption locates at around 450nm.

The SERS spectra were obtained with the wavenumbers ranged from 400 cm^{-1} to 1800 cm^{-1} by a confocal Raman microscope (HR Evolution, Horiba JY, France). A 785nm diode laser was used as the excitation source, and the SERS spectra were collected with a 20x microscope objective lens (NA = 0.40). The integration time was set to 10 s, and the spectral resolution was 1 cm^{-1}. Each sample was repeatedly measured five times at different locations, including center and edge, and the average spectrum of those five SERS measurements was used for further processing and analysis.

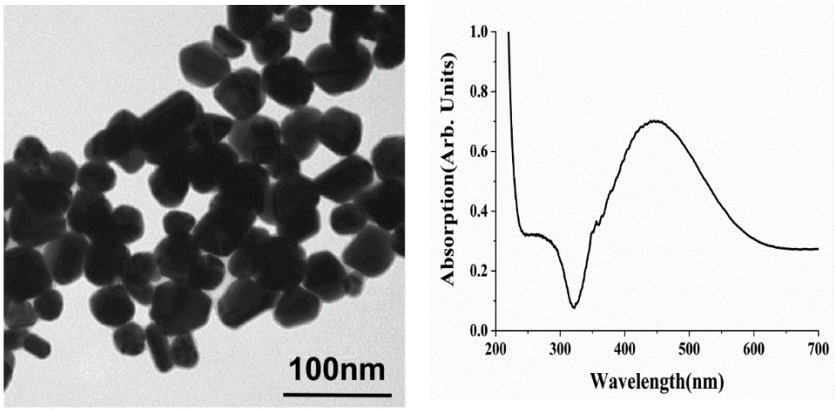

Fig. 1. The TEM micrograph of the concentrated silver colloid mixed with blood serum (Left) and the UV/visible absorption spectrum of the silver colloid (Right).

2.2 SERS data preprocessing and analysis

The SERS spectra were smoothed by Savitzky-Golay algorithm [30] to reduce the noise, and the fluorescence background was subsequently estimated by the fifth order polynomial fitting and removed from the original SERS spectra [31]. In order to alleviate the impact of the variations of Raman peak intensities among different blood serum samples, normalization was performed on each SERS spectrum after fluorescence background removal by dividing the Raman intensity at each wavenumber by the summation of the Raman intensities at all wavenumbers. Hence, only the relative Raman intensities have been taken into account rather than the absolute Raman intensities in this study.

PLS analysis [32], as a dimension reduction methodology, was employed to compress the spectral data and the first twenty PLS components (PC) and PC scores were extracted from all the blood serum Raman measurements after preprocessing. Thereafter, the number of selected PC scores was optimized from the first PC score until the first twenty PC scores to achieve better classification performance. More specifically, a two-step scheme classification was conducted to first differentiate blood serum SERS spectra into the bladder cancer group and healthy group. Then, a second step was further performed to classify those blood serum SERS spectra in the bladder cancer group into NMIBC group and MIBC group. The two-step scheme can improve the overall classification accuracy by selecting optimal differentiators in each step, i.e. the optimal number of selected PC scores. In order to evaluate the proposed method in an unbiased manner, leave-one-out cross-validation (LOOCV) method was performed on all SERS data [33]. More specifically, an average spectrum corresponding to one subject was selected as the test data and the remaining spectra corresponding to the other subjects were served as the training data until all the spectra (or subjects) were tested once. To further evaluate the performance of the PLS-LDA classification model, the ROC curves were generated and the integrated area under the ROC curves (AUC) was used as a quantitative indicator to represent the classifier performance [34,35].

Biomedical Optics EXPRESS

3. Results and discussions

3.1 Evaluating the enhancement effect of silver colloid

In order to verify the enhancement effect of the silver colloid, SERS spectrum and spontaneous Raman spectrum of the same blood serum sample, Raman spectrum of silver colloid and Raman spectrum of aluminum foil are collected under the exactly same configuration. The Raman intensities in many dominant vibrational bands of SERS spectrum are enhanced dramatically compared to those of spontaneous Raman spectrum, and none obvious Raman peak is observed in the Raman measurements of silver colloid and aluminum foil, as shown in Fig. 2. Therefore, there should be interactions between the silver nanoparticles and the blood serum, in which some of the basic biochemical substances of blood serum, such as protein and nucleic acid, are being adsorbed onto silver nanoparticles, leading to a significant enhancement of Raman signal. By such a method, only 2μl blood serum is sufficient to collect optimal SERS measurements, which may benefit its clinical applications in bladder cancer diagnosis.

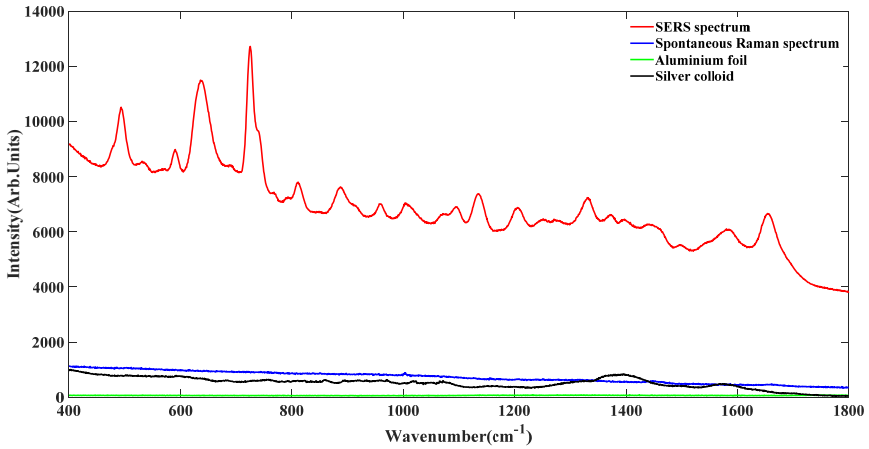

Fig. 2. The comparison of SERS spectrum and spontaneous Raman spectrum of the same blood serum sample, Raman spectrum of silver colloid and Raman spectrum of aluminum foil.

3.2 Biochemical changes of blood serum samples among healthy, NMIBC and MIBC groups

Figure 3(a) shows the average blood serum SERS spectra after fluorescence background removal and normalization from healthy, NMIBC and MIBC groups respectively. It can be seen that the primary differences of SERS peak intensities between healthy and bladder cancer samples are at 494, 589, 639, 725, 812, 887, 1004, 1073, 1093, 1135, 1206, 1330, 1443, 1581 and 1654cm^{-1}, which can be assigned to different vibrational modes and biochemicals (as listed in Table 1) according to the previously published studies [36–38]. Furthermore, significant differences of SERS spectra can also be observed between healthy, NMIBC and MIBC groups, respectively. It can be seen from Fig. 3 that the L-arginine (494cm^{-1}), amide-VI (589cm^{-1}), L-tyrosine (639cm^{-1}), amide-I and α-Helix (1654 cm^{-1}) exhibit more intense Raman signals in MIBC group compared with those in the healthy and NMIBC groups. These findings suggest that an increase of free amino acids presents in patients' blood serum during the malignancy development, which is consistent with the results in the previous studies [39,40]. The reason might be that abnormal vigorous growth and proliferation of tumor cells require abundant nutrients and energy, leading to the disorder of amino acid metabolism [41], thus increased amino acids are likely a comprehensive effect of the protein catabolism [42], the degradation of extracellular matrix and the autophagic

Biomedical Optics EXPRESS

degradation of preexisting intracellular proteins [43,44]. In addition, it is obvious that the peak at 725cm^{-1} increased substantially in both NMIBC and MIBC groups compared to that in the healthy group. This Raman peak corresponds to the C-H bending vibration mode of adenine, indicating the abnormal metabolism of DNA and RNA bases in the blood serum of bladder cancer patients [37]. Some studies have reported that the DNA concentration in blood serum is higher in many types of tumors [45,46], and the concentration of cell-free DNA in the blood serum typically increases with tumor progression [47], which may result from the necrosis or apoptosis of tumor cells and the release of highly proliferating tumor cells [46]. The larger Raman peak of D-mannos (1135cm^{-1}) in the MIBC group demonstrates more saccharide in blood serum, which might be due to the disordered glycolysis via the tricarboxylic acid cycle [48]. The Raman peak at 1443cm^{-1} corresponding to saturated fatty acids decreases or even disappears in MIBC group, because the rapid tumor cells proliferation consumes a large amount of fatty acids to fulfill the demand of cell membrane synthesis and energy production [49]. Thus, the depletion of serum fatty acids suggests that the lipids play important roles in tumor pathogenesis [50]. Based on the above results, there are significant changes of biomolecules in different blood serum groups, thus blood serum SERS demonstrates great potential for identifying healthy, NMIBC and MIBC individuals.

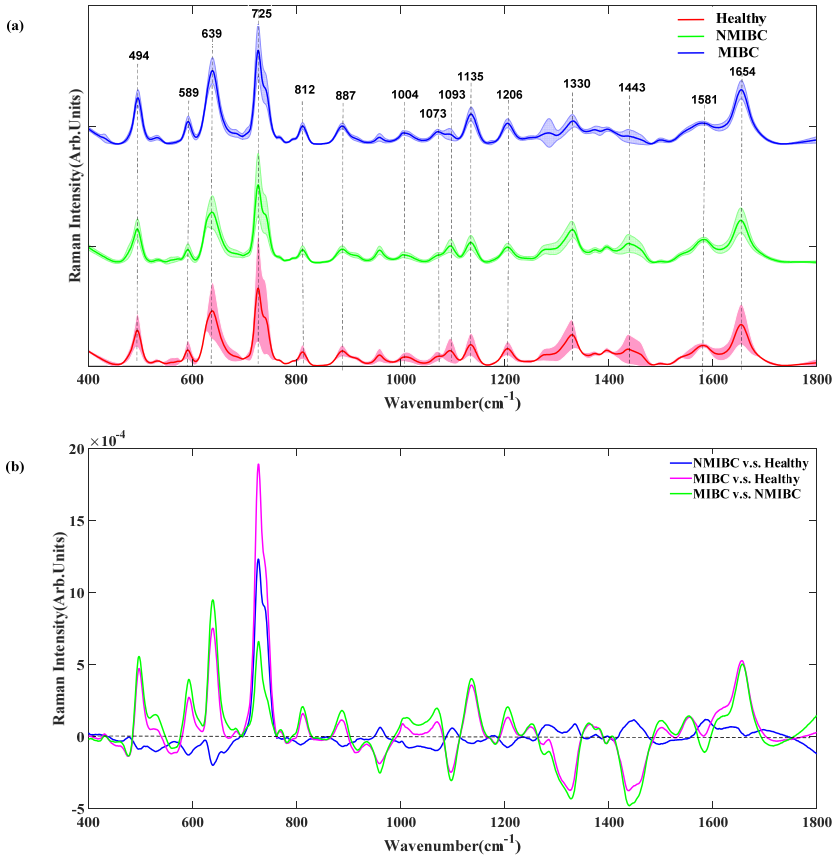

Fig. 3. (a) The average SERS spectra after fluorescence background removal and normalization from the healthy, NMIBC and MIBC groups, in which the shaded areas represent the standard deviations among each group; (b) the subtracted spectra between different groups.

Biomedical Optics EXPRESS

Table 1. The Assignments of the Raman Peaks with Significant Differences among Healthy, NMIBC and MIBC Groups

Peak position (cm^{-1})	Assignments
494	Ring vibration, Cellulose, guanine, L-arginine
589	Ascorbic acid, amide-VI
639	C-S stretching vibration, L-Tyrosine, lactose
725	C-H bending vibration, Adenine, coenzyme A
812	C-C-O stretching vibration, L-Serine, glutathione
887	C-O-H bending vibration, Glutathione, D-(C)-galactosamine
1004	C-C symmetric stretch, Phenylalanine
1073	C-N stretching vibration, Collagen
1093	C-N stretching vibration, D-Mannos
1135	C-N stretching vibration, D-Mannos
1206	Ring vibration, L-Tryptophan, Phenylalanine
1330	C-H stretching vibration, Nucleic acid bases, D-mannos
1443	CH2 bending vibration, Glycine, L-Proline, stearic acid
1581	C = C bending vibration, Phenylalanine, acetoacetate, riboflavin
1654	C = O stretching vibration, amide-I, α-Helix

3.3 Analysis of the SERS spectra

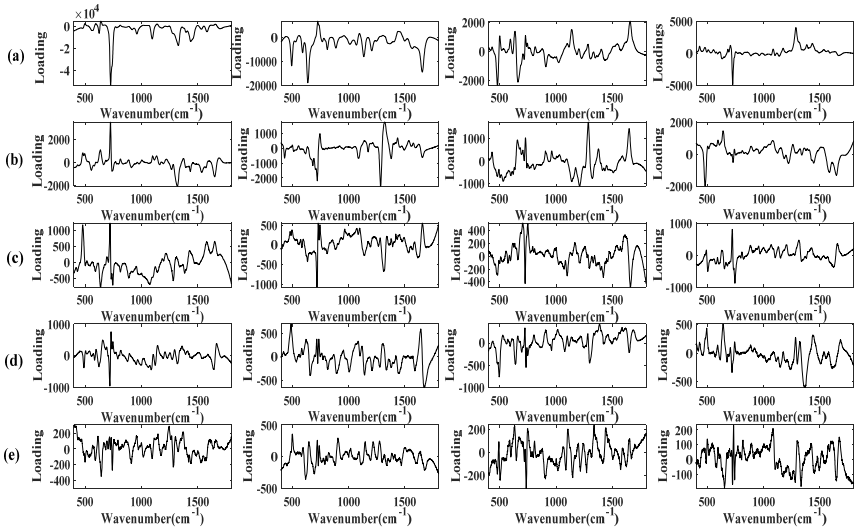

Fig. 4. The first twenty PLS components of blood serum SERS spectra: (a) PC 1 to 4 (from left to right); (b) PC 5 to 8 (from left to right); (c) PC 9 to 12 (from left to right); (d) PC 13 to 16 (from left to right); (e) PC 17 to 20 (from left to right).

The first twenty PLS components and PC scores are derived from 90 blood serum SERS spectra based on PLS analysis, and those PLS components are shown in Fig. 4. It can be observed that the peaks in those PLS components are in good agreement with the differences of Raman spectra among each group as shown in Fig. 3(b), especially for the first several PLS components. Thus, the PLS components are expected to capture the most information about the differences of Raman spectra among each group. In addition, three PC scores with most statistically significant differences are selected by Wilcoxon rank-sum test and plotted in Fig. 5(a) and (b), i.e., PC1 ($p = 0.0032$), PC3 ($p<0.0001$) and PC5 ($p = 0.0036$) are selected for healthy and bladder cancer groups; and PC1 ($p = 0.0006$), PC6 ($p = 0.0331$) and PC8 ($p<0.0001$) are selected for NMIBC and MIBC groups; in which the PC scores of each group tend to be concentrated within certain regions. It can be observed that the bladder cancer group shows more extensive distribution than the healthy group in the PC scores scatter plot,

Biomedical Optics EXPRESS

which is in good agreement with the results previously reported in paper [20]. The reason might be that the proportions of the components, e.g. protein, lipids and glucose, are relatively stable in blood serum of healthy people whereas they vary among different cancer patients due to the heterogeneity of cancer progress [20]. Furthermore, the linear discriminant scores for the final classification are plotted in Fig. 5(c) and (d). These linear discriminant scores are derived from the PC scores based on LDA model and excellent separation among different groups can be observed.

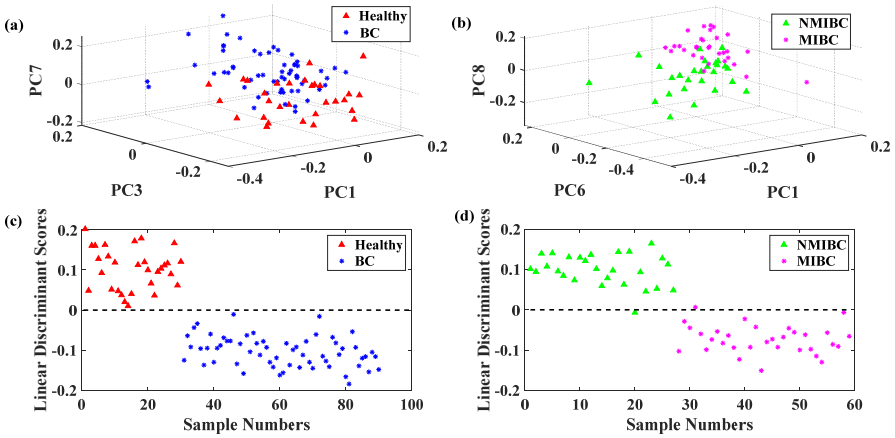

Fig. 5. 3D scatter plot of PC scores of (a) healthy and bladder cancer groups, (b) NMIBC and MIBC groups; Scatter plot of the linear discriminant scores of (c) healthy and bladder cancer groups, (d) NMIBC and MIBC groups.

Table 2 shows the overall classification results of the two-step binary classification method. The bladder cancer group was treated as positive while the healthy group was treated as negative in the first binary classification, and MIBC group was treated as positive while the NMIBC group was treated as negative in the second binary classification. More specifically, 29 of 30 spectra in the healthy group and 59 of 60 spectra in the bladder cancer group are accurately classified in the first binary classification with the accuracy, sensitivity and specificity of 97.8%, 98.3% and 96.7%, respectively. In the second binary classification, 26 of 27 spectra from the NMIBC group and 29 of 32 spectra from the MIBC group are accurately identified with the accuracy, sensitivity and specificity of 93.2%, 90.6% and 96.3%, respectively. Thus, the overall classification accuracy reaches 93.3% for identifying healthy, NMIBC and MIBC groups, which is much higher compared to that of conventional clinical examinations, such as cystoscopy and bladder imaging. According to the ROC curves in Fig. 6, the AUC values are 0.987 and 0.983 for healthy versus bladder cancer groups and NMIBC versus MIBC groups, respectively. Such large integration areas further confirm the excellent classification performance of the proposed method. Therefore, the SERS technique combined with PLS-LDA algorithm based on serum samples has great potential for accurately identifying healthy, NMIBC and MIBC patients with high sensitivity and specificity.

Biomedical Optics EXPRESS

Table 2. The Overall Classification Results of Healthy, NMIBC and MIBC Groups

Method	Group	Predicted group			Total
		Healthy	NMIBC	MIBC	
PLS-LDA count (%)	Healthy	29(96.7%)	1(3.3%)	0(0%)	30(100%)
	NMIBC	1(3.6%)	26(92.8%)	1(3.6%)	28(100%)
	MIBC	0(0%)	3(9.4%)	29(90.6%)	32(100%)

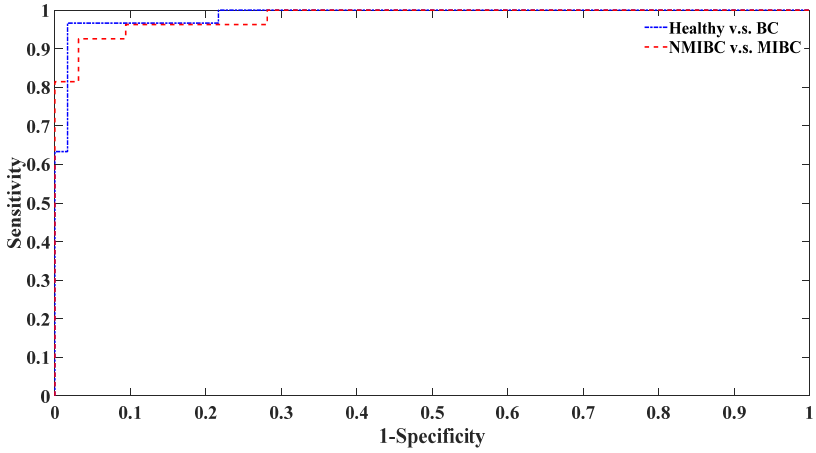

Fig. 6. The ROC curves obtained by using PLS-LDA based classification model between healthy and bladder cancer groups, and between NMIBC and MIBC groups.

4. Conclusions

In this study, SERS measurements on a small volume of blood serum are used to identify healthy, NMIBC and MIBC patients. Biochemical changes, such as the levels of proteins, nucleic acids, saccharide and lipids, are observed among different groups, which should be closely relevant to the protein catabolism, cell proliferation and metabolic alterations in blood serum during bladder cancer progression. By combining with the PLS-LDA method, high classification accuracy, sensitivity and specificity can be achieved based on the blood serum SERS measurements. The excellent performance of this method has demonstrated its potential for fast, accurate, and noninvasive assessment of muscle invasion of bladder cancer. Thus, rational therapy plans can be made timely, and the survival rate can be improved significantly.

Funding

National Natural Science Foundation of China (61605025); Fund for Innovative Research Groups of the National Natural Science Foundation of China (71621061); Science and Technology Foundation of National Defense Key Laboratory (61424080209); Program for Innovation Talents in Universities of Liaoning Province (LR2016031); Ningbo Natural Science Foundation (2018A610365); Fundamental Research Funds for the Central Universities (N171902001, N171904006); the 111 Project (B16009).

Disclosures

The authors declare that there are no conflicts of interest related to this article.

Biomedical Optics EXPRESS

References

1. S. Antoni, J. Ferlay, I. Soerjomataram, A. Znaor, A. Jemal, and F. Bray, "Bladder Cancer Incidence and Mortality: A Global Overview and Recent Trends," Eur. Urol. **71**(1), 96–108 (2017).
2. F. Bray, J. Ferlay, I. Soerjomataram, R. L. Siegel, L. A. Torre, and A. Jemal, "Global cancer statistics 2018: GLOBOCAN estimates of incidence and mortality worldwide for 36 cancers in 185 countries," CA Cancer J. Clin. **68**(6), 394–424 (2018).
3. B. W. G. van Rhijn, M. Burger, Y. Lotan, E. Solsona, C. G. Stief, R. J. Sylvester, J. A. Witjes, and A. R. Zlotta, "Recurrence and progression of disease in non-muscle-invasive bladder cancer: from epidemiology to treatment strategy," Eur. Urol. **56**(3), 430–442 (2009).
4. Z. Kirkali, T. Chan, M. Manoharan, F. Algaba, C. Busch, L. Cheng, L. Kiemeney, M. Kriegmair, R. Montironi, W. M. Murphy, I. A. Sesterhenn, M. Tachibana, and J. Weider, "Bladder cancer: epidemiology, staging and grading, and diagnosis," Urology **66**(6 Suppl 1), 4–34 (2005).
5. M. S. Soloway, "Diagnosis and management of superficial bladder cancer," Semin. Surg. Oncol. **5**(4), 247–254 (1989).
6. B. P. Schrier, M. P. Hollander, B. W. van Rhijn, L. A. Kiemeney, and J. A. Witjes, "Prognosis of muscle-invasive bladder cancer: difference between primary and progressive tumours and implications for therapy," Eur. Urol. **45**(3), 292–296 (2004).
7. P. Mariappan, V. Lavin, C. Q. Phua, S. A. A. Khan, R. Donat, and G. Smith, "Predicting grade and stage at cystoscopy in newly presenting bladder cancers-a prospective double-blind clinical study," Urology **109**, 134–139 (2017).
8. A. D. MacVicar, "Bladder cancer staging," BJU Int. **86**(Suppl 1), 111–122 (2000).
9. N. P. DeFelippo, R. P. Fortunato, H. Z. Mellins, and J. P. Richie, "Intravenous urography: important adjunct for diagnosis of bladder tumours," Br. J. Urol. **56**(5), 502–505 (1984).
10. J. O. Salo, L. Kivisaari, and T. Lehtonen, "Comparison of magnetic resonance imaging with computed tomography and intravesical ultrasound in staging bladder cancer," Urol. Radiol. **10**(4), 167–172 (1988).
11. J. E. Husband, J. F. Olliff, M. P. Williams, C. W. Heron, and G. R. Cherryman, "Bladder cancer: staging with CT and MR imaging," Radiology **173**(2), 435–440 (1989).
12. N. Lawrentschuk, S. T. Lee, and A. M. Scott, "Current role of PET, CT, MR for invasive bladder cancer," Curr. Urol. Rep. **14**(2), 84–89 (2013).
13. A. Tekes, I. Kamel, K. Imam, G. Szarf, M. Schoenberg, K. Nasir, R. Thompson, and D. Bluemke, "Dynamic MRI of bladder cancer: evaluation of staging accuracy," AJR Am. J. Roentgenol. **184**(1), 121–127 (2005).
14. M. Takeuchi, S. Sasaki, T. Naiki, N. Kawai, K. Kohri, M. Hara, and Y. Shibamoto, "MR imaging of urinary bladder cancer for T-staging: a review and a pictorial essay of diffusion-weighted imaging," J. Magn. Reson. Imaging **38**(6), 1299–1309 (2013).
15. L. T. Kerr, K. Domijan, I. Cullen, and B. M. Hennelly, "Applications of Raman spectroscopy to the urinary bladder for cancer diagnostics," Photonics Lasers Med. **3**(3), 193–224 (2014).
16. A. C. Goh and S. P. Lerner, "Application of new technology in bladder cancer diagnosis and treatment," World J. Urol. **27**(3), 301–307 (2009).
17. M. I. Toma, M. G. Friedrich, S. H. Hautmann, K. T. Jäkel, A. Erbersdobler, A. Hellstern, and H. Huland, "Comparison of the ImmunoCyt test and urinary cytology with other urine tests in the detection and surveillance of bladder cancer," World J. Urol. **22**(2), 145–149 (2004).
18. F. Ye, L. Wang, M. Castillo-Martin, R. McBride, M. D. Galsky, J. Zhu, P. Boffetta, D. Y. Zhang, and C. Cordon-Cardo, "Biomarkers for bladder cancer management: present and future," Am. J. Clin. Exp. Urol. **2**(1), 1–14 (2014).
19. K. Kong, C. Kendall, N. Stone, and I. Notingher, "Raman spectroscopy for medical diagnostics--From in-vitro biofluid assays to in-vivo cancer detection," Adv. Drug Deliv. Rev. **89**, 121–134 (2015).
20. S. Feng, R. Chen, J. Lin, J. Pan, G. Chen, Y. Li, M. Cheng, Z. Huang, J. Chen, and H. Zeng, "Nasopharyngeal cancer detection based on blood plasma surface-enhanced Raman spectroscopy and multivariate analysis," Biosens. Bioelectron. **25**(11), 2414–2419 (2010).
21. D. Cialla, A. März, R. Böhme, F. Theil, K. Weber, M. Schmitt, and J. Popp, "Surface-enhanced Raman spectroscopy (SERS): progress and trends," Anal. Bioanal. Chem. **403**(1), 27–54 (2012).
22. S. Nie and S. R. Emory, "Probing Single Molecules and Single Nanoparticles by Surface-Enhanced Raman Scattering," Science **275**(5303), 1102–1106 (1997).
23. E. C. Le Ru, E. Blackie, M. Meyer, and P. G. Etchegoin, "Surface Enhanced Raman Scattering Enhancement Factors: A Comprehensive Study," J. Phys. Chem. C **111**(37), 13794–13803 (2007).
24. G. Wang, R. J. Lipert, M. Jain, S. Kaur, S. Chakraboty, M. P. Torres, S. K. Batra, R. E. Brand, and M. D. Porter, "Detection of the potential pancreatic cancer marker MUC4 in serum using surface-enhanced Raman scattering," Anal. Chem. **83**(7), 2554–2561 (2011).
25. S. Li, L. Li, Q. Zeng, Y. Zhang, Z. Guo, Z. Liu, M. Jin, C. Su, L. Lin, J. Xu, and S. Liu, "Characterization and noninvasive diagnosis of bladder cancer with serum surface enhanced Raman spectroscopy and genetic algorithms," Sci. Rep. **5**(1), 9582 (2015).
26. Y. Zhang, X. Ping, Q. Zeng, L. Li, L. Lin, S. Li, Z. Liu, C. Su, M. Qi, and Z. Guo, "Classifying low-grade and high-grade bladder cancer using label-free serum surface-enhanced Raman spectroscopy and support vector machine," Laser Phys. **28**(3), 035603 (2018).

Biomedical Optics EXPRESS

27. P. C. Lee and D. Meisel, "Adsorption and Surface-Enhanced Raman of Dyes on Silver and God Sols," J. Phys. Chem. **86**(17), 3391–3395 (1982).
28. K. Liu and S. F. Wu, "Silver colloid synthesized by microwave method and applied in Surface Enhanced Raman Scattering," J. Light Scattering **14**(7), 332–335 (2006).
29. M. Si, Y. Kang, and Z. Zhang, "Surface-enhanced Raman scattering (SERS) spectra of chloramphenicol in Ag colloids prepared by microwave heating method," J. Raman Spec. **40**(9), 1319–1323 (2009).
30. S. Chen, X. Lin, C. Yuen, S. Padmanabhan, R. W. Beuerman, and Q. Liu, "Recovery of Raman spectra with low signal-to-noise ratio using Wiener estimation," Opt. Express **22**(10), 12102–12114 (2014).
31. S. Chen, L. Kong, W. Xu, X. Cui, and Q. Liu, "A Fast Fluorescence Background Suppression Method for Raman Spectroscopy Based on Stepwise Spectral Reconstruction," IEEE Access **6**, 67709–67717 (2018).
32. S. Chen, C. Zhu, C. Hoe-Kong Chui, G. Sheoran, B. K. Tan, and Q. Liu, "Spectral diffuse reflectance and autofluorescence imaging can perform early prediction of blood vessel occlusion in skin flaps," J. Biophotonics **10**(12), 1665–1675 (2017).
33. G. S. Wasserman and H. Mohsen, "Computer intensive statistical methods: validation, model selection and bootstrap," J. Qual. Technol. **27**(3), 268–270 (1995).
34. S. Zhu, X. Cui, W. Xu, S. Chen, and W. Qian, "Weighted Spectral Reconstruction Method for Discrimination of Bacteria Species with Low Signal-to-Noise Ratio Raman Measurements," RSC Advances **9**(17), 9500–9508 (2019).
35. T. Fawcett, "An introduction to roc analysis," Pattern Recognit. Lett. **27**(8), 861–874 (2006).
36. H. W. Han, X. L. Yan, R. X. Dong, G. Ban, and K. Li, "Analysis of serum from type ii diabetes mellitus and diabetic complication using surface-enhanced Raman spectra (SERS)," Appl. Phys. B **94**(4), 667–672 (2009).
37. J. D. Gelder, K. D. Gussem, P. Vandenabeele, and L. Moens, "Reference database of Raman spectra of biological molecules," J. Raman Spectrosc. **38**(9), 1133–1147 (2007).
38. J. Lin, R. Chen, S. Feng, J. Pan, Y. Li, G. Chen, M. Cheng, Z. Huang, Y. Yu, and H. Zeng, "A novel blood plasma analysis technique combining membrane electrophoresis with silver nanoparticle-based SERS spectroscopy for potential applications in noninvasive cancer detection," Nanomedicine (Lond.) **7**(5), 655–663 (2011).
39. K. Dettmer, F. C. Vogl, A. P. Ritter, W. Zhu, N. Nürnberger, M. Kreutz, P. J. Oefner, W. Gronwald, and E. Gottfried, "Distinct metabolic differences between various human cancer and primary cells," Electrophoresis **34**(19), 2836–2847 (2013).
40. P. Tripathi, B. S. Somashekar, M. Ponnusamy, A. Gursky, S. Dailey, P. Kunju, C. T. Lee, A. M. Chinnaiyan, T. M. Rajendiran, and A. Ramamoorthy, "HR-MAS NMR tissue metabolomic signatures cross-validated by mass spectrometry distinguish bladder cancer from benign disease," J. Proteome Res. **12**(7), 3519–3528 (2013).
41. B. J. Altman and C. V. Dang, "Normal and cancer cell metabolism: lymphocytes and lymphoma," FEBS J. **279**(15), 2598–2609 (2012).
42. J. M. Argilés and J. Azcón-Bieto, "The metabolic environment of cancer," Mol. Cell. Biochem. **81**(1), 3–17 (1988).
43. A. Hirayama, K. Kami, M. Sugimoto, M. Sugawara, N. Toki, H. Onozuka, T. Kinoshita, N. Saito, A. Ochiai, M. Tomita, H. Esumi, and T. Soga, "Quantitative metabolome profiling of colon and stomach cancer microenvironment by capillary electrophoresis time-of-flight mass spectrometry," Cancer Res. **69**(11), 4918–4925 (2009).
44. W. Dröge, "Autophagy and aging--importance of amino acid levels," Mech. Ageing Dev. **125**(3), 161–168 (2004).
45. S. J. Dawson, D. W. Y. Tsui, M. Murtaza, H. Biggs, O. M. Rueda, S. F. Chin, M. J. Dunning, D. Gale, T. Forshew, B. Mahler-Araujo, S. Rajan, S. Humphray, J. Becq, D. Halsall, M. Wallis, D. Bentley, C. Caldas, and N. Rosenfeld, "Analysis of Circulating tumor DNA to monitor metastatic breast cancer," N. Engl. J. Med. **368**(13), 1199–1209 (2013).
46. C. Bettegowda, M. Sausen, R. J. Leary, I. Kinde, Y. Wang, N. Agrawal, B. R. Bartlett, H. Wang, B. Luber, R. M. Alani, E. S. Antonarakis, N. S. Azad, A. Bardelli, H. Brem, J. L. Cameron, C. C. Lee, L. A. Fecher, G. L. Gallia, P. Gibbs, D. Le, R. L. Giuntoli, M. Goggins, M. D. Hogarty, M. Holdhoff, S. M. Hong, Y. Jiao, H. H. Juhl, J. J. Kim, G. Siravegna, D. A. Laheru, C. Lauricella, M. Lim, E. J. Lipson, S. K. Marie, G. J. Netto, K. S. Oliner, A. Olivi, L. Olsson, G. J. Riggins, A. Sartore-Bianchi, K. Schmidt, M. Shih, S. M. Oba-Shinjo, S. Siena, D. Theodorescu, J. Tie, T. T. Harkins, S. Veronese, T. L. Wang, J. D. Weingart, C. L. Wolfgang, L. D. Wood, D. Xing, R. H. Hruban, J. Wu, P. J. Allen, C. M. Schmidt, M. A. Choti, V. E. Velculescu, K. W. Kinzler, B. Vogelstein, N. Papadopoulos, and L. A. Diaz, Jr., "Detection of circulating tumor DNA in early- and late-stage human malignancies," Sci. Transl. Med. **6**(224), 224ra24 (2014).
47. L. Xue, B. Yan, Y. Li, Y. Tan, X. Luo, and M. Wang, "Surface-enhanced Raman spectroscopy of blood serum based on gold nanoparticles for tumor stages detection and histologic grades classification of oral squamous cell carcinoma," Int. J. Nanomedicine **13**, 4977–4986 (2018).
48. H. Song, J. S. Peng, Y. Dong-Sheng, Z. L. Yang, H. L. Liu, Y. K. Zeng, X. P. Shi, and B. Y. Lu, "Serum metabolic profiling of human gastric cancer based on gas chromatography/mass spectrometry," Braz. J. Med. Biol. Res. **45**(1), 78–85 (2012).
49. F. P. Kuhajda, "Fatty Acid Synthase and Cancer: New Application of an Old Pathway," Cancer Res. **66**(12), 5977–5980 (2006).

Biomedical Optics EXPRESS

50. J. A. Menendez and R. Lupu, "Fatty acid synthase and the lipogenic phenotype in cancer pathogenesis," Nat. Rev. Cancer **7**(10), 763–777 (2007).